NANO LETTERS

Letter

pubs.acs.org/NanoLett

Spontaneous Internalization of Cell Penetrating Peptide-Modified Nanowires into Primary Neurons

Jae-Hyun Lee,[†] Anqi Zhang,[†] Siheng Sean You,[†] and Charles M. Lieber*[,†,‡]

[†]Department of Chemistry and Chemical Biology and [‡]John A. Paulson School of Engineering and Applied Science, Harvard University, Cambridge, Massachusetts 02138, United States

Supporting Information

ABSTRACT: Semiconductor nanowire (NW) devices that can address intracellular electrophysiological events with high sensitivity and spatial resolution are emerging as key tools in nanobioelectronics. Intracellular delivery of NWs without compromising cellular integrity and metabolic activity has, however, proven difficult without external mechanical forces or electrical pulses. Here, we introduce a biomimetic approach in which a cell penetrating peptide, the trans-activating transcriptional activator (TAT) from human immunodeficiency virus 1, is linked to the surface of Si NWs to facilitate spontaneous internalization of NWs into primary neuronal cells. Confocal microscopy imaging studies at fixed time points demonstrate that TAT-conjugated NWs (TAT-NWs) are fully internalized into mouse hippocampal neurons, and quantitative image analyses reveal an ca. 15% internalization efficiency. In addition, live cell dynamic imaging of NW internalization shows that NW penetration begins within 10−20 min after binding to the membrane and that NWs become fully internalized within 30−40 min. The generality of cell penetrating peptide modification method is further demonstrated by internalization of TAT-NWs into primary dorsal root ganglion (DRG) neurons.

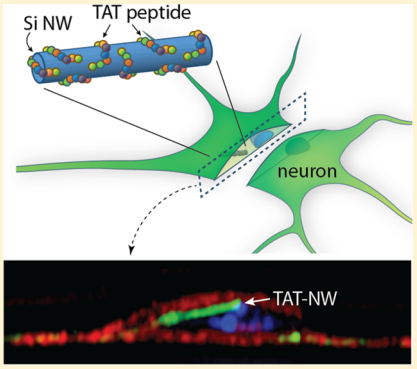

KEYWORDS: *Silicon nanowires, surface modification, TAT peptide transfection, hippocampal neurons, dorsal root ganglion cells, live cell confocal imaging, membrane penetration*

The application of nanomaterials in bioelectronics,[1] including ultrasensitive sensing,[2−6] single-cell electrophysiological probes,[7−12] flexible, stretchable, and/or degradable electronics,[13−15] and macroporous three-dimensional electronics[16,17] have enabled research ranging from disease marker detection[5] to cell electrophysiology[11] and brain mapping.[18] Surface modification of nanodevices is well-established in the area of sensing where linkage of receptors is crucial for selective detection,[5] but also represents a critical challenge for creating bio−nano interfaces that are stable at the cellular level. For example, internalization of Si NW devices across the cell membrane in cardiac cells has demonstrated the capability for nanoscale sensing elements to record intracellular action potentials without compromising cell viability.[7−9] Similar results have been difficult to achieve in neuronal systems, where the capability to detect stable full-amplitude intracellular action potentials without interference from the cell membrane, could open up unique research opportunities.

To date, the use of NWs for interrogating the intracellular environment of neurons has been limited by challenges in achieving stable internalization of the highly anisotropic NW devices. A limited number of approaches have been reported for the internalization of highly anisotropic NWs in neurons, with an emphasis on physical methods.[10,19−23] Specifically, neurons were cultured on substrates with vertical NW arrays, which delivered biomolecules to the cytoplasm as a result of gravity and/or adhesive force driven internalization,[19] and electroporation was used to achieve transient access to intracellular action potentials.[10] Concurrently, these same physical strategies have been used in a variety of other cell types to demonstrate internalization of vertical NW[8,24,25]/nanotube arrays[26−29] or single NWs[30] into the cells.

In another approach, chemically based alteration of the cell membrane and subsequent NW internalization has been achieved by treating Chinese hamster ovary cells with the polar organic solvent dimethyl sulfoxide (DMSO).[31] Given that the typical size of NWs used in electronic devices is comparable to large macromolecules, viruses, and nanoparticles, it is reasonable to ask whether a biomimetic strategy used for targeted delivery of these structures might be developed for driving internalization of NWs. Indeed, surface modification of Si NW devices with cell membrane-like phospholipids has been shown to be effective in inducing internalization of the NWs into cardiac cells and enabling intracellular recording of stable action potentials.[7,9] However, successful application of this biomimetic approach has not yet been reported for the internalization of NWs into neurons.

Here, we demonstrate a new strategy for complete internalization of NWs into neurons using cell penetrating peptides (CPPs). CPPs are short peptides capable of delivering cargo into cells.[32] TAT peptide is a well-known CPP derived

Received: January 3, 2016
Published: January 8, 2016

DOI: 10.1021/acs.nanolett.6b00020
Nano Lett. 2016, 16, 1509−1513

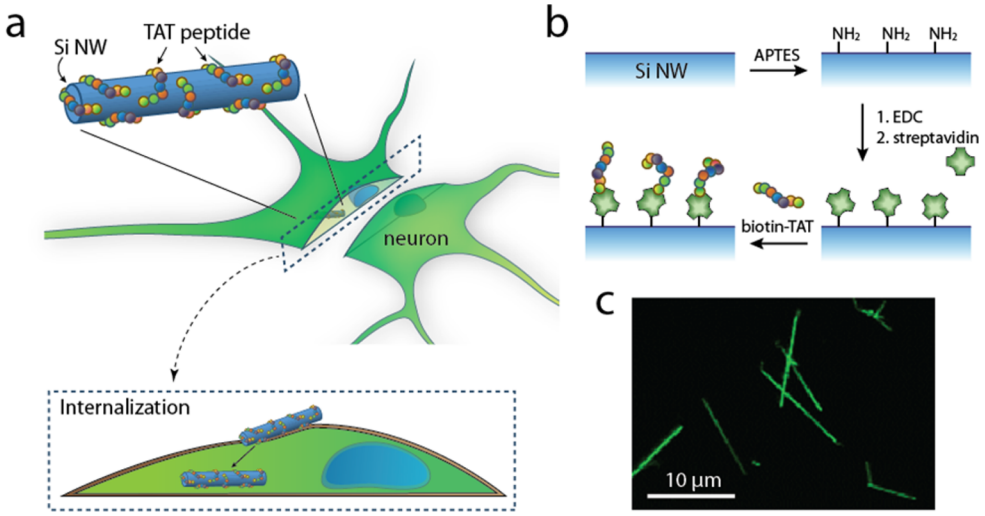

Figure 1. (a) Schematic of internalization of TAT peptide modified Si NW into neuron. (b) Conjugation scheme of TAT to the surface of Si NW. Streptavidin (STV) is first covalently attached via EDC coupling reaction. Biotin-TAT peptide is then conjugated onto the STV. (c) Fluorescence microscope image of TAT-NWs labeled with STV-Alexa Fluor 555 conjugate.

from HIV-1[33] and is effective at delivering materials of various sizes including small molecules (Å),[34] nucleic acids (nm),[35,36] proteins (a few to tens of nanometers)[37,38] and submicron particles[39] into primary cells (e.g., neurons) and immortalized cell lines. Freestanding Si NWs conjugated with TAT CPPs show complete internalization into mouse hippocampal neurons with a yield of ∼15%. Confocal microscopy revealed that the internalization is spontaneous, without additional mechanical force or electroporation. Studies of the internalization process by live cell confocal microscopy imaging demonstrate that the NWs are completely internalized within 30−40 min after initial attachment to the cell membrane. In addition, our studies show that TAT-NWs can also be internalized into DRG cells, a peripheral neuron type, suggesting the generality of our TAT CPP approach for driving NW internalization into primary neurons.

An overview of our strategy is shown in Figure 1a. TAT-modified Si NWs are delivered to a culture of neuronal cells; the NW-cell mixture is incubated for a fixed time, and then confocal microscopy is used to analyze the positions of NWs with respect to the cell membrane. At the chosen time points, confocal microscopy images are recorded at different distances relative to the substrate surface with distinct fluorescent labels for the NWs, cell membranes, and cell nuclei, and then NW positions are analyzed relative to the membrane surface in either a 3D top- or cross-sectional views (see Supporting Information for details).

TAT modification of Si NWs was achieved by the strategy outlined in Figure 1b (see Supporting Information for details). First, Si NWs (*n*-doped, 80 nm in diameter and ca. 10 μm in length) were synthesized by the gold nanocluster catalyzed vapor−liquid−solid method.[40] Second, the NWs on the growth substrate were modified with (3-aminopropyl)-triethoxysilane (APTES) to yield a primary amine-terminated monolayer.[41] Third, Alexa Fluor 555 labeled streptavidin (STV) was covalently coupled to NWs using 1-ethyl-3-(3-(dimethylamino)propyl) carbodiimide (EDC). Fourth, the STV-modified NW (STV-NW) substrate was incubated in biotin-TAT solution for binding. The resulting TAT-conjugated Si NWs (TAT-NWs) were detached from the substrate by brief sonication before use. A representative fluorescence microscopy image of TAT-NWs dispersed on a glass substrate (Figure 1c) exhibits constant fluorescence along the NW long axes consistent with uniform STV (TAT) modification.

Schematics of NW interface with neuronal membrane are shown in Figure 2a, where TAT peptides on the NW interact

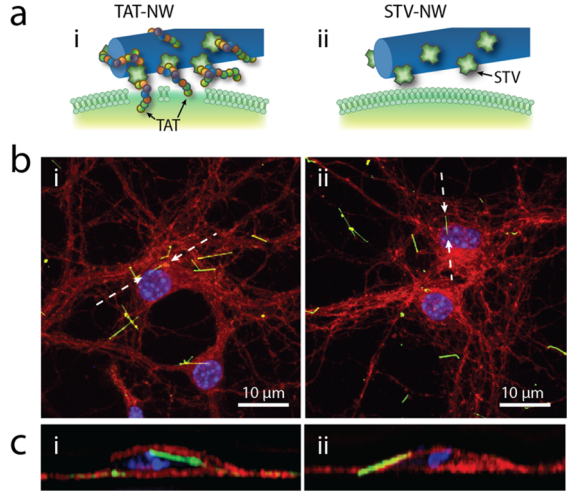

Figure 2. (a) Schematics of (i) TAT-NW and (ii) STV-NW interacting with the cell membrane. (b) Confocal microscope *z*-stack images of (i) TAT-NWs and (ii) STV-NWs dispersed onto hippocampal neurons. Each image consists of a stack of 29 0.5 μm thick confocal images. (c) *Z*-section images along the white dashed lines in (b). Red: cell membrane (WGA-Alexa 597); green: NWs (Alexa 555); blue: nucleus (Hoechst 33258).

with the membrane and facilitate spontaneous NW internalization (Figure 2a,i) while STV-NW, which does not have CPPs, remains on the membrane outer surface (Figure 2a,ii). Initial trials of cell internalization were carried out by dispersing TAT-NWs (5 μg) onto mouse hippocampal neurons, and incubating for 20 h at 37 °C; prior to the TAT-NW addition, the neurons were cultured for 2 weeks. As a control, STV-NWs without TAT conjugation were dispersed in a similar manner on a separate neuron culture and incubated for 20 h. After

DOI: 10.1021/acs.nanolett.6b00020
Nano Lett. 2016, 16, 1509−1513

fixation, the cells were labeled with WGA-Alexa Fluor 594 for membrane staining and Hoechst 33258 for nuclei staining, and the samples were imaged by confocal microscopy (see Supporting Information for details). Representative *z*-stack confocal microscopy images of these two distinct sample types (Figure 2b) resolve clearly labeled NWs (green), neuron cell membranes (red) and nuclei (blue). To determine unambiguously the positions of NWs in these *z*-stacks, we analyzed cross sections taken along the NW long axes. Representative cross sections (Figure 2c) along NWs marked by the white dashed lines in Figure 2b show unambiguously that the TAT-NW was fully internalized without affecting neuronal membrane integrity (Figure 2c,i), while the STV-NW was not internalized (Figure 2c,ii).

The positions of individual NWs can be well-determined by the above analysis of cross sections of the confocal *z*-stack images (Figure 2c), although this method is inefficient for statistical analyses such as the overall internalization yield. To more efficiently determine whether or not NWs are internalized across an entire sample image, we use the surface reconstruction method illustrated in Figure 3a with key features as follows. *Z*-stack confocal microscopy images are acquired (Figure 3a,i), and then an image of the cell surface is reconstructed (Figure 3a,ii), where NWs above the cell surface are also visible. This image is then compared to the corresponding NW fluorescence channel (Figure 3a,iii) to unambiguously assign NWs internalized or external to the cells in the image. For example, the surface reconstruction in Figure 3a shows only part of NW 2 (Figure 3a,ii), and thus we can assign NWs 1 and 3 visible in the NW fluorescence channel (Figure 3a,iii) as internalized.

A comparison between the reconstructed images (Figure 3b, top row) and NW channels (Figure 3b, middle row) shows that the NWs marked with white arrowheads were internalized. To validate the assigned internalization of these NWs we also carried out cross-section analyses (Figure 3b, bottom row), which demonstrate clearly that the positions of the three NWs were in the interior of the neuron soma. The advantage of surface analysis is that one single wide field image is sufficient to assess the positions of a large number of NWs (Supporting Information, Figure S1). First, plots of the number of cumulative internalized NWs for 50 randomly selected NWs (Supporting Information, Figure S1d) show further that the internalization numbers were consistent for both methods. Second, large-area assessment of all of the TAT-NWs by the surface reconstruction method (Figure 3c) show that after 20 h of incubation 51/342 NWs were internalized, an internalization yield of 14.9%. Further analysis of these data as a function of NW length (Figure 3c) yields similar mean values for the internalized and total NWs: 4.1 and 4.8 μm, respectively. Last, similar measurements and analyses carried out for TAT-NW incubation times of 6 and 32 h (Supporting Information, Figure S2) resulted in internalization rates of 10.9 and 14.1%, respectively. These results suggest that the majority of internalization events occur within the first 6 h for the hippocampal neurons.

To better understand the dynamics of TAT-NW internalization process, we carried out in situ live cell confocal imaging. The imaging chamber (Figure 4a; see Supporting Information for details) was designed for an upright microscope and utilized a hole in the top of a cell culture Petri dish to allow access of a water immersion objective lens, with the chamber fixed on a heating plate to maintain a constant temperature of 37 °C. The

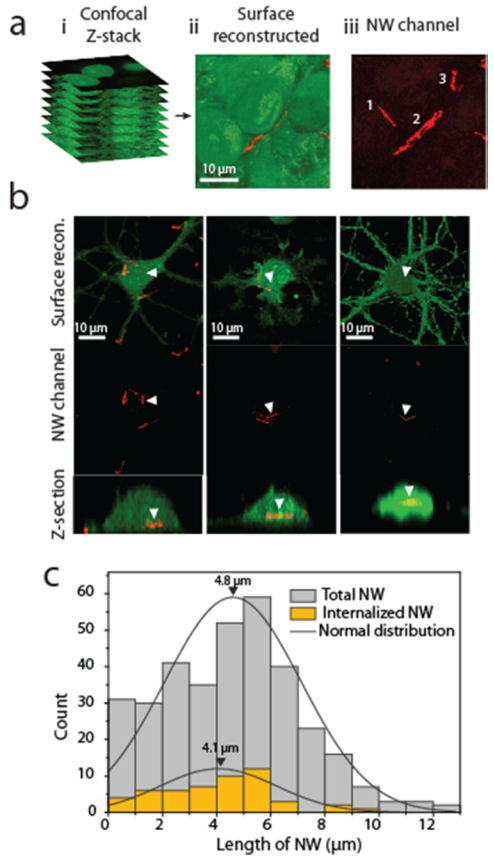

Figure 3. Image analysis of TAT-NW internalization into mouse hippocampal neurons. (a) Workflow of assessing NW internalization. The cell surface is reconstructed from confocal *z*-stack images using Volume Viewer in ImageJ, NIH, and is compared with NW fluorescence channel. The sample image shows NW1 and 3 are internalized, and NW2 is on the membrane surface. Green: cytosol (calcein); red: NW (Alexa 555). (b) More neuron images with internalized TAT-NWs (white arrowheads). Top: surface reconstructed image; middle: NW fluorescence channel; bottom: confocal *z*-section image on NW. (c) Histogram of total NWs and internalized NWs vs NW length. Black lines correspond to normal distribution fits, and the arrow heads indicate mean NW length values.

chamber was kept in a cell culture incubator between every imaging session, and the $x-y$ location markers on the bottom of the imaging chamber enabled the determination of the exact position of a target cell for up to 10 time point measurements without reducing cell viability (Figure 4b).[42]

Initial low-resolution experiments (20× objective) monitoring of TAT-NW internalization were carried out with imaging at hourly time points to determine the time scale regime of the internalization dynamics. Significantly, the relative positions of TAT-NWs determined from cross-section analyses (e.g., Supporting Information, Figure S3) showed that internalization can occur during the first hour. More detailed high-resolution (100× objective) imaging studies with a 10 min imaging interval (Figure 4c and d) demonstrate several key points. First, TAT-NWs begin to cross the neuronal cell membrane within only 10−20 min after initial attachment. Second, internalization is complete for the characterized NWs within 30−40 min. Third, the STV-NWs maintain constant positions on the cell membrane indicating that there is no internalization over this same period of time. Last, following internalization we monitored cell viability using calcein-AM (see Supporting

DOI: 10.1021/acs.nanolett.6b00020
Nano Lett. 2016, 16, 1509−1513

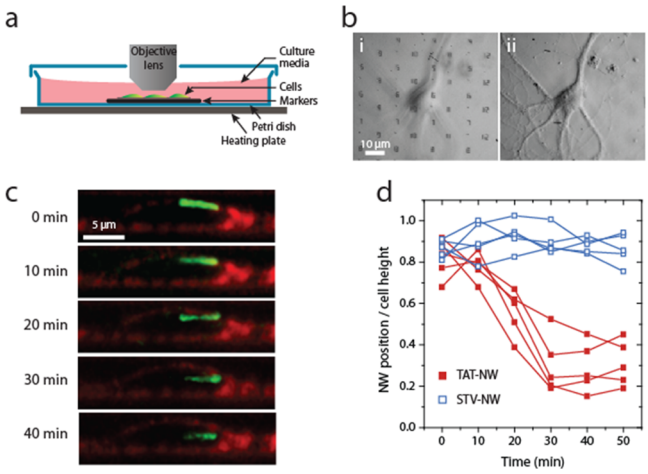

Figure 4. Real-time imaging of TAT-NW internalization. (a) Schematic of imaging chamber used for live cell imaging. The chamber has a marker region at the bottom for locating the cell of interest. (b) Bright field images of neuron on markers with focal plane on (i) the markers and (ii) the neuron. (c) Temporal cross-section confocal images. Neuronal membrane is stained with WGA-Alexa 594 (red) and TAT-NW is stained with Alexa 555 (green). All images are the same size, with scale bar as indicated in the 0 min image. (d) Temporal changes of the relative positions of TAT-NWs and STV-NWs (control); $N = 5$ for each NW type.

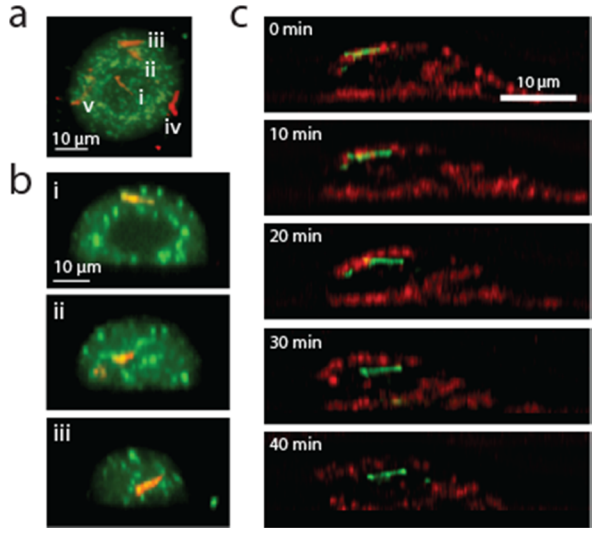

Figure 5. TAT-NW internalization into a DRG cell. (a) Confocal microscope z-stack image (a stack of 48 0.5 μm thick confocal images) of a DRG cell with TAT-NWs following 20 h incubation. Green: cytosol (calcein), red: NW (Alexa 555). (b) Cross-section images of NWs (i–iii) in (a) along the NW long axes. (c) Temporal cross-section confocal images. Red: plasma membrane (WGA-Alexa 594), Green: NW (Alexa 555). All images are the same size, with the scale bar as indicated in the 0 min image.

Information for details) and found 97% fluorescence intensity was retained after 3 h, thus indicating that NW internalization has a minimal influence on cell activity/viability on this time scale.

To test the generality of TAT-NW internalization in primary neurons, the same internalization method was investigated for DRG cells. The DRG cells were isolated from rat spinal cord and kept at 4 °C for 2 days prior to the NW internalization experiments (see Supporting Information for details). TAT-NWs were dispersed onto the DRG culture, and the cells were incubated for 20 h at 37 °C. Figure 5a shows a representative z-stack confocal image of a fixed DRG cell where the labeled TAT-NWs (red, i–v) are clearly resolved. Cross sections taken along the long axes of NWs i–iii (Figure 5b) show unambiguously that these NWs are fully internalized on the 20 h time scale of the incubation. To assess the internalization dynamics, we further carried out live cell confocal microscopy studies as described above for the hippocampal neurons. Cross-section analyses of images recorded with a 10 min interval (Figure 5c) reveal that the TAT-NW internalization initiated ca. 10 min following NW binding to the membrane and was completed within 30 min; these results are thus similar to our observations for hippocampal neurons.

Together our imaging results show clearly that TAT-modification of NWs leads to internalization in primary neurons. In addition, these results indicate that the entry angle of TAT-NWs into these cells was <10° and that perpendicular entry was not observed. Our results are consistent with the general mechanism for cell-penetrating peptides such as TAT.[43,44] Specifically, the mechanism of TAT-mediated translocation is reported to be via penetration of cell membrane by the TAT peptide,[43,44] and thus the uniformly modified TAT-NWs should not have a preference for entry angle. Importantly, we suggest that these results for TAT-NWs could be applied in future studies to internalization of TAT-modified kinked-NW nanoelectronic probes[7,9] to facilitate intracellular recording from neurons.

In conclusion, we have introduced a biomimetic approach in which the TAT CPP is linked to the surface of Si NWs to facilitate spontaneous internalization of NWs into primary neuronal cells. Confocal microscopy imaging studies at fixed time points demonstrate that TAT-NWs fully internalize into mouse hippocampal neurons, and quantitative image analyses reveal an ca. 15% internalization efficiency. In addition, live cell dynamic imaging of NW internalization process has shown that NW penetration begins within 10–20 min after binding to the membrane, and that NWs become fully internalized within 30–40 min. The generality of CPP modification method was further demonstrated by internalization of TAT-NWs into primary DRG neurons. Significantly, this biomimetic internalization approach is expected to be applicable to semiconductor NW devices that are emerging as biosensors and powerful cellular probes[1−10] and thus should enable recording of intracellular potentials and biochemical signals in a highly localized and targeted manner in the future.

■ ASSOCIATED CONTENT

Supporting Information

The Supporting Information is available free of charge on the ACS Publications website at DOI: 10.1021/acs.nanolett.6b00020.

Detailed methods and additional figures about synthesis of Si NWs, TAT peptide conjugation, culturing hippocampal neurons and dissecting DRG cells, imaging chamber fabrication, quantification of NW internalization, and live cell confocal imaging of NW internalization process (PDF)

DOI: 10.1021/acs.nanolett.6b00020
Nano Lett. 2016, 16, 1509−1513

AUTHOR INFORMATION

Corresponding Author

*E-mail: cml@cmliris.harvard.edu.

Author Contributions

J.-H.L., A.Z., and S.Y. contributed equally to this work.

Notes

The authors declare no competing financial interest.

ACKNOWLEDGMENTS

We thank Dr. Jinlin Huang for helpful discussion and assistance with imaging chamber design, and Dr. Pin Liu and Prof. Bruce Bean for help with the dissection technique used to obtain DRG cells. C.M.L. acknowledges support of this work by the Air Force Office of Scientific Research. J.-H.L acknowledges support from Basic Science Research Program through the National Research Foundation of Korea (2013R1A6A3A03062506).

REFERENCES

(1) Zhang, A.; Lieber, C. M. *Chem. Rev.* **2015**, DOI: 10.1021/acs.chemrev.5b00608.
(2) Cui, Y.; Wei, Q.; Park, H.; Lieber, C. M. *Science* **2001**, *293*, 1289−1292.
(3) Zheng, G.; Patolsky, F.; Cui, Y.; Wang, W. U.; Lieber, C. M. *Nat. Biotechnol.* **2005**, *23*, 1294−1301.
(4) Misra, N.; Martinez, J. A.; Huang, S.-C. J.; Wang, Y.; Stroeve, P.; Grigoropoulos, C. P.; Noy, A. *Proc. Natl. Acad. Sci. U. S. A.* **2009**, *106*, 13780−13784.
(5) Patolsky, F.; Lieber, C. M. *Mater. Today* **2005**, *8*, 20−28.
(6) Chen, K.-I.; Li, B.-R.; Chen, Y.-T. *Nano Today* **2011**, *6*, 131−154.
(7) Tian, B.; Cohen-Karni, T.; Qing, Q.; Duan, X.; Xie, P.; Lieber, C. M. *Science* **2010**, *329*, 830−834.
(8) Xie, C.; Lin, Z.; Hanson, L.; Cui, Y.; Cui, B. *Nat. Nanotechnol.* **2012**, *7*, 185−190.
(9) Qing, Q.; Jiang, Z.; Xu, L.; Gao, R.; Mai, L.; Lieber, C. M. *Nat. Nanotechnol.* **2013**, *9*, 142−147.
(10) Robinson, J. T.; Jorgolli, M.; Shalek, A. K.; Yoon, M.-H.; Gertner, R. S.; Park, H. *Nat. Nanotechnol.* **2012**, *7*, 180−184.
(11) Duan, X.; Fu, T.-M.; Liu, J.; Lieber, C. M. *Nano Today* **2013**, *8*, 351−373.
(12) Spira, M. E.; Hai, A. *Nat. Nanotechnol.* **2013**, *8*, 83−94.
(13) Takei, K.; Takahashi, T.; Ho, J. C.; Ko, H.; Gillies, A. G.; Leu, P. W.; Fearing, R. S.; Javey, A. *Nat. Mater.* **2010**, *9*, 821−826.
(14) Lipomi, D. J.; Vosgueritchian, M.; Tee, B. C.; Hellstrom, S. L.; Lee, J. A.; Fox, C. H.; Bao, Z. *Nat. Nanotechnol.* **2011**, *6*, 788−792.
(15) Jeong, J.-W.; Shin, G.; Park, S. I.; Yu, Ki J.; Xu, L.; Rogers, J. A. *Neuron* **2015**, *86*, 175−186.
(16) Tian, B.; Liu, J.; Dvir, T.; Jin, L.; Tsui, J. H.; Qing, Q.; Suo, Z.; Langer, R.; Kohane, D. S.; Lieber, C. M. *Nat. Mater.* **2012**, *11*, 986−994.
(17) Liu, J.; Fu, T.-M.; Cheng, Z.; Hong, G.; Zhou, T.; Jin, L.; Duvvuri, M.; Jiang, Z.; Kruskal, P.; Xie, C.; Suo, Z.; Fang, Y.; Lieber, C. M. *Nat. Nanotechnol.* **2015**, *10*, 629−636.
(18) Alivisatos, A. P.; Andrews, A. M.; Boyden, E. S.; Chun, M.; Church, G. M.; Deisseroth, K.; Donoghue, J. P.; Fraser, S. E.; Lippincott-Schwartz, J.; Looger, L. L.; Masmanidis, S.; McEuen, P. L.; Nurmikko, A. V.; Park, H.; Peterka, D. S.; Reid, C.; Roukes, M. L.; Scherer, A.; Schnitzer, M.; Sejnowski, T. J.; Shepard, K. L.; Tsao, D.; Turrigiano, G.; Weiss, P. S.; Xu, C.; Yuste, R.; Zhuang, X. *ACS Nano* **2013**, *7*, 1850−1866.
(19) Shalek, A. K.; Robinson, J. T.; Karp, E. S.; Lee, J. S.; Ahn, D.-R.; Yoon, M.-H.; Sutton, A.; Jorgolli, M.; Gertner, R. S.; Gujral, T. S.; MacBeath, G.; Yang, E. G.; Park, H. *Proc. Natl. Acad. Sci. U. S. A.* **2010**, *107*, 1870−1875.
(20) Yoon, I.; Hamaguchi, K.; Borzenets, I. V.; Finkelstein, G.; Mooney, R.; Donald, B. R. *PLoS One* **2013**, *8*, e65715.
(21) Ferguson, J. E.; Boldt, C.; Puhl, J. G.; Stigen, T. W.; Jackson, J. C.; Crisp, K. M.; Mesce, K. A.; Netoff, T. I.; Redish, A. D. *Nanomedicine* **2012**, *7*, 847−853.
(22) Hanson, L.; Lin, Z. C.; Xie, C.; Cui, Y.; Cui, B. *Nano Lett.* **2012**, *12*, 5815−5820.
(23) Kwiat, M.; Elnathan, R.; Pevzner, A.; Peretz, A.; Barak, B.; Peretz, H.; Ducobni, T.; Stein, D.; Mittelman, L.; Ashery, U.; Patolsky, F. *ACS Appl. Mater. Interfaces* **2012**, *4*, 3542−3549.
(24) Shalek, A. K.; Gaublomme, J. T.; Wang, L.; Yosef, N.; Chevrier, N.; Andersen, M. S.; Robinson, J. T.; Pochet, N.; Neuberg, D.; Gertner, R. S.; Amit, I.; Brown, J. R.; Hacohen, N.; Regev, A.; Wu, C. J.; Park, H. *Nano Lett.* **2012**, *12*, 6498−6504.
(25) Mumm, F.; Beckwith, K. M.; Bonde, S.; Martinez, K. L.; Sikorski, P. *Small* **2013**, *9*, 263−272.
(26) VanDersarl, J. J.; Xu, A. M.; Melosh, N. A. *Nano Lett.* **2012**, *12*, 3881−3886.
(27) Xu, A. M.; Aalipour, A.; Leal-Ortiz, S.; Mekhdjian, A. H.; Xie, X.; Dunn, A. R.; Garner, C. C.; Melosh, N. A. *Nat. Commun.* **2014**, *5*, 3613.
(28) Lin, Z. C.; Xie, C.; Osakada, Y.; Cui, Y.; Cui, B. *Nat. Commun.* **2014**, *5*, 3206.
(29) Xie, X.; Aalipour, A.; Gupta, S. V.; Melosh, N. A. *ACS Nano* **2015**, *9*, 11667−11677.
(30) Zimmerman, J. F.; Murray, G. F.; Wang, Y.; Jumper, J. M.; Austin, J. R.; Tian, B. *Nano Lett.* **2015**, *15*, 5492−5498.
(31) Aalipour, A.; Xu, A. M.; Leal-Ortiz, S.; Garner, C. C.; Melosh, N. A. *Langmuir* **2014**, *30*, 12362−12367.
(32) Copolovici, D. M.; Langel, K.; Eriste, E.; Langel, Ü. *ACS Nano* **2014**, *8*, 1972−1994.
(33) Frankel, A. D.; Pabo, C. O. *Cell* **1988**, *55*, 1189−1193.
(34) Polyakov, V.; Sharma, V.; Dahlheimer, J. L.; Pica, C. M.; Luker, G. D.; Piwnica-Worms, D. *Bioconjugate Chem.* **2000**, *11*, 762−771.
(35) Moschos, S. A.; Jones, S. W.; Perry, M. M.; Williams, A. E.; Erjefalt, J. S.; Turner, J. J.; Barnes, P. J.; Sproat, B. S.; Gait, M. J.; Lindsay, M. A. *Bioconjugate Chem.* **2007**, *18*, 1450−1459.
(36) Astriab-Fisher, A.; Sergueev, D.; Fisher, M.; Shaw, B. R.; Juliano, R. *Pharm. Res.* **2002**, *19*, 744−754.
(37) Schwarze, S. R.; Ho, A.; Vocero-Akbani, A.; Dowdy, S. F. *Science* **1999**, *285*, 1569−1572.
(38) Wadia, J. S.; Stan, R. V.; Dowdy, S. F. *Nat. Med.* **2004**, *10*, 310−315.
(39) Mao, Z.; Wan, L.; Hu, L.; Ma, L.; Gao, C. *Colloids Surf., B* **2010**, *75*, 432−440.
(40) Morales, A. M.; Lieber, C. M. *Science* **1998**, *279*, 208−211.
(41) Hermanson, G. T. Chapter 13 - Silane Coupling Agents. In *Bioconjugate Techniques*, 3rd ed.; Hermanson, G. T., Ed.; Academic Press: Boston, 2013; pp 535−548.
(42) Hanson, L.; Cui, L.; Xie, C.; Cui, B. *Microsc. Res. Tech.* **2011**, *74*, 496−501.
(43) Ciobanasu, C.; Siebrasse, J. P.; Kubitscheck, U. *Biophys. J.* **2010**, *99*, 153−162.
(44) Mishra, A.; Lai, G. H.; Schmidt, N. W.; Sun, V. Z.; Rodriguez, A. R.; Tong, R.; Tang, L.; Cheng, J.; Deming, T. J.; Kamei, D. T. *Proc. Natl. Acad. Sci. U. S. A.* **2011**, *108*, 16883−16888.

DOI: 10.1021/acs.nanolett.6b00020
Nano Lett. 2016, 16, 1509−1513